HHS Public Access

Author manuscript

Health Phys. Author manuscript; available in PMC 2015 October 22.

Published in final edited form as:

Health Phys. 2012 October ; 103(4): 454–462.

Development and dosimetry of a small animal lung irradiation platform

Ross McGurk[a], **Caroline Hadley**[b], **Isabel L. Jackson**[c], and **Zeljko Vujaskovic, MD, PhD**[a,b,c]

[a]Medical Physics Graduate Program, Duke University Medical Center, Durham, NC 27710

[b]Department of Radiation Oncology, Duke University Medical Center, Durham, NC 27710

[c]Department of Pathology, Duke University Medical Center, Durham, NC 27710

Abstract

Advances in large scale screening of medical counter measures for radiation-induced normal tissue toxicity are currently hampered by animal irradiation paradigms that are both inefficient and highly variable among institutions. Here, we introduce a novel high-throughput small animal irradiation platform for use in orthovoltage small animal irradiators. We used radiochromic film and metal oxide semiconductor field effect transistor detectors to examine several parameters, including 2D field uniformity, dose rate consistency, and shielding transmission. We posit that this setup will improve efficiency of drug screens by allowing for simultaneous, targeted irradiation of multiple animals, improving efficiency within a single institution. Additionally, we suggest that measurement of the described parameters in all centers conducting counter measure studies will improve the translatability of findings among institutions.

We also investigated the use of tissue equivalent phantoms in performing dosimetry measurements for small animal irradiation experiments. Though these phantoms are commonly used in dosimetry, we recorded a significant difference in both the entrance and target tissue dose rates between euthanized rats and mice with implanted detectors and the corresponding phantom measurement. This suggests that measurements using these phantoms may not provide accurate dosimetry for *in vivo* experiments.

Based on these measurements, we propose that this small animal irradiation platform can increase the capacity of animal studies by allowing for more efficient animal irradiation. We also suggest that researchers fully characterize the parameters of whatever radiation setup is in use in order to facilitate better comparison among institutions.

Keywords

small-animal dosimetry; radiochromic film; MOSFET; x-rayirradiation

Corresponding author. Zeljko Vujaskovic, MD, PhD, Professor, Departments of Radiation Oncology and Pathology; Medical Physics Program, Box 3455 MSRB, Duke University Medical Center, Durham, NC 27710, P: +1 919 681 1675, F: +1 919 681 2651.

The authors declare no conflict of interest.

Introduction

Following the formation of the Weapons of Mass Destruction Medical Countermeasures Subcommittee, a working group was established to identify what the goals of medical countermeasures research should be to further national preparedness for a possible radiological or nuclear threat (Pellmar and Rockwell 2005). The resulting report includes many objectives for researchers, one of which is establishing an improved animal model of radiation injury to permit rapid testing of proposed countermeasures (Stone et al. 2004, Pellmar and Rockwell 2005). Much of the work in this area has focused on the identification of animals whose radiation response is most analogous to that of humans (Coleman et al. 2004, Augustine et al. 2005). Small animal models, which allow for larger numbers of animals to be studied in a shorter time frame and at lower cost than larger animals, are of particular interest (Williams et al. 2010). Currently, one of the confounding factors of radiation countermeasure development is the variation in radiation methods and parameters among facilities, making it difficult to compare findings from multiple institutions (Yoshizumi et al. 2011).

A necessary part of developing small animal models is the creation of a method of delivering radiation that can mimic therapeutic or accidental radiation exposure to a specific region or organ, for our purposes, the lung. Currently, several different systems of focused small animal irradiation are in use (Verhaegen et al. 2011). These systems vary in configuration but generally involve a specialized platform used to guide delivery of the desired radiation dose to a specific region of a single animal with (Wong et al. 2008, Zhou et al. 2010, Clarkson et al. 2011) or without (Stojadinovic et al. 2007) the aid of an integrated imaging system.

Specialized, single animal commercial systems allow for accurate delivery of radiation, but may not be sufficient to keep pace with the growing demand for screening of potential medical countermeasures for normal tissue radiation injury. High throughput screenings of potential therapeutic agents will likely involve multiple facilities and large groups of animals (Stone et al. 2004). For this reason, it is necessary to develop multi-animal irradiation setups, the parameters of which are well characterized, so that the resultant findings at one institution can be compared with those from other groups. The resulting improved comparisons will allow for better characterization of the radiobiological effect as well as more accurate assessments of the relative efficacy of proposed therapeutic countermeasures (Yoshizumi et al. 2011).

In pursuit of this goal, we have developed a novel small animal irradiation platform (SAIP), capable of simultaneously irradiating 12 mice or 4 rats, and have characterized its performance when used with conventional x-ray irradiators. Using radiochromic film and metal oxide semiconductor field effect transistor (MOSFET) detectors, both established metrics for animal and phantom irradiation (Scarantino et al. 2004, De Lin et al. 2008, Ngwa et al. 2011), we first investigated the field uniformity, dose rate consistency, and shielding transmission factors of this setup. Following this technical validation, we went on to measure entrance and target tissue dose rates in both traditional phantoms and euthanized

animals with implanted detectors. From these studies we were able to identify differences between phantom and in-animal measurements, as well as in entrance versus target tissues.

The push to develop medical countermeasures to radiation injury demands an increase in the number and power of small animal radiation studies. This will involve multi-site studies, meaning that there must be a standardization of radiation delivery across facilities in order to ensure optimal and comparable results. While some technical aspects of this paper are similar to studies by Ngwa et al. (Ngwa et al. 2011), Wong et al. (Wong et al. 2008) and Newton et al. (Newton et al. 2011), here we introduce a platform that increases the number of animals able to be irradiated simultaneously, as well as a set of parameters that, if measured across facilities, would allow for better comparison of findings among studies. We submit that these findings will improve the efficiency, accuracy, and reliability of small animal models for radiation research.

MATERIALS AND METHODS

Irradiation Platform

Our new small-animal irradiation platform (SAIP) consists of a series of acrylic dividers to aide in animal immobilization and moveable 8 mm thick lead shielding blocks mounted on stainless steel guides (Figure 1). The half value layer (HVL) of lead for a 320 kVp monoenergetic x-ray beam is approximately 1.7 mm (Berger et al. 1998). Therefore given the beam effective energy of a 320 kVp beam is much lower, shielding transmission is expected to be less than 3%. Regardless, additional shielding can be added easily if required. Importantly, we increase the number of animals able to be placed in the field of our previous SAIP to12 mice, or 4 rats from 4 and 1, respectively. Further, these mice and rats can be positioned such that thoracic, abdominal, and whole brain irradiation is possible, greatly increasing the utility of the platform.

X-ray equipment

There are two XRAD 320 kilovoltage irradiation systems at our institution (Precision X-Ray Inc., North Branford, CT). The first irradiator (Irradiator A) has the ability to deliver 5 kV – 320 kV in 0.1 kV increments. At the maximum tube potential of 320 kV, the x-ray tube current can be set to a maximum of 12.5 milliamps (mA). The second system (Irradiator B) differs in that at the maximum tube voltage of 320 kV, the maximum tube current is 10 mA. All calibration and dose rate measurements were performed at 320 kVp tube voltage and 10 mA tube current with 2 mm aluminum added filtration. Further, both units contain a shelf to allow animals to be positioned at a source-to-surface distance (SSD) of 50 cm. The shelf can also be removed completely to provide a maximum SSD of 75 cm. The maximum field size at a SSD of 50 cm is 20×20 cm^2 but at 75 cm SSD this is enlarged to 30×30 cm^2 due to beam divergence.

MOSFET dosimetry system and calibration

The dose measurements were made with a mobile MOSFET system (Model TN-RD-70-W, Best Medical Canada, Ottawa, Canada) as previously described (De Lin et al. 2008). Our method differs in that we used the standard sensitivity model (TN-1002RD) MOSFET

detectors rather than the high sensitivity bias MOSFET detectors (TN-502aRD) because of the large cumulative doses being delivered to each detector. MOSFET calibration was done at an SSD of 75 cm. For each experiment MOSFET detectors from the same batch were used. For each experiment MOSFET detectors from the same batch were used. Each detector was calibrated using the manufacturer specified procedure where MOSFET readings are calibrated against absolute dose measurements from an ionization chamber whose calibration factor was determined by the Accredited Dosimetry Calibration Lab (ADCL) at the University of Wisconsin for 250 kVp x-rays. This is the highest tube voltage for which there was an available calibration factor. The error in using this correction factor instead of the one for 320 kVp is expected to be less than 1% due to the small variation in correction factor in the kilovoltage energy range for a given cylindrical ion chamber (Ma et al. 2001).

Field uniformity

Field uniformity was tested using a sheet of radiochromic film (XR-RV3 GAFCHROMIC®, International Specialty Products, Wayne, NJ) cut to size (16×18 cm^2) to fit the area in which animals are positioned on the platform during irradiation. Film image acquisition was done according to the procedure outlined by Newton et al (Newton et al. 2011). In more detail, films were pre-scanned using a Hewlett Packard Scanjet G3110 (Hewlett Packard, Palo Alto, CA) or Epson Expression 1000×L (Epson America Inc., Long Beach, CA) desktop scanner at 150 dpi and saved in the tagged-image-file format (TIF) (McLaughlin et al. 1991). Each film was scanned three times to produce an average image. Films were then exposed for 3 minutes with 320 kVp and 10 mA tube current. No shielding was in place for this irradiation. After irradiation, films were stored in darkness for approximately 24-hours post-irradiation to ensure the optical density (OD) had stabilized. The pre-irradiated scan was subtracted from the post-irradiated film to provide a 2D change in OD image. A 10×10 median filter was used to smooth electronic noise. Two normalizations strategies were used. First, for isocontour visualization, each filtered image was normalized to the maximum PV. Normalizing to the maximum is justified since the film has been shown to have a near linear dose response for total doses of between 1 and 5 Gy (Blair and Meyer 2009). Second, using the first normalization, a rectangular region of interest (ROI) was created using the minimum and maximum extents of the 80% isocontour in the horizontal and vertical directions and PVs were normalized to the mean value within this ROI. The maximum, minimum and standard deviation of these normalized PVs was calculated to quantify variation throughout the field.

Dose rate investigations

A series of measurements were acquired to answer the following questions. One, does the dose rate change over long irradiation times (e.g. irradiation times one order of magnitude longer than used for MOSFET calibration)? Two, is there difference in lung dose rate measured in phantom versus animal lung cavities? Three, is there a difference in measured lung dose rates between irradiators? Four, what is the difference between surface and lung dose rates? Finally, what is the reduction in dose rates due to shielding?

For animal experiments we euthanized the animals and implanted detectors into the thoracic cavity or placed them on the skin. For phantom measurements a tissue equivalent mouse or rat phantom (CIRS, Norfolk, VA) was used with the detectors placed in a drilled cavity approximating the location of the thoracic cavity. Detectors and readout cables were secured with surgical tape and their placement confirmed by acquiring port films with irradiator settings of 120 kVp, 30 mA tube current and 5 minute beam on time which provided sufficient soft tissue contrast to allow the visualization of the animal outline and lungs and the detectors within. The x-ray tube setting used for calibration and field uniformity testing was set and depending on the experiment, either a 30 second, or one minute beam-on time, followed by an individual dose readout was performed three times to find the average dose rate for that detector.

The first series of measurements tested the dose rate consistency of both irradiators over the required irradiation times calculated to deliver 10 Gy based on the prior 30 second or 1 minute dose rate measurements. Detectors were placed in the thoracic cavities of the tissue equivalent mouse phantom and three euthanized C57BL/6J mice (Jackson Laboratory, Bar Harbor, ME). Animals were equally spaced across the field on one side of the platform with the phantom placed in the center of the field on the opposite side (Figure 2A). One minute lung dose rates were recorded for a field width of 1.5 cm (cranial-caudal direction) and averaged to compute the time necessary to deliver 10 Gy (Figure 2B). This time was then set and the radiation delivered. The percent difference between the total dose averaged overall detectors and the planned 10 Gy dose was calculated. For Irradiator B, we repeated the above procedure by measuring the lung dose rate in another three euthanized C57BL/6J mice (but no phantom) and without shielding.

The second series of measurements involved gathering data for investigating the remaining four questions. The first experiment used the same mice, equipment and arrangement as the dose rate consistency experiment on Irradiator A described above. Field widths of 1, 1.5, and 2.0 cm were defined by positioning the shield to define the radiation field width in the cranial-caudal direction (Figure 2B). Dose rates were also recorded without any lead shielding present (Figure 2A). The experiment was then repeated on Irradiator B to show that consistent results from experiments could be expected, regardless of which irradiator was used. However, for this experiment an additional two MOSEFT detectors were used. The first was placed on the skin of one mouse to acquire surface dose rate measurements and the second being placed on the hind leg of a second mouse and which remained fully shielded throughout the experiment.

Finally, the third series of measurements repeated the second series of measurements but with the tissue equivalent rat phantom and two Wistar rats (Charles River Labs, Wilmington, MA) and only on Irradiator B. As in the case of the second series of measurements, two additional detectors were used in addition to the detectors in the thoracic cavities. One was placed on the phantom surface and the second was placed on the skin of one rat for surface dose rate measurements (Figure 2C). Dose rate measurements were acquired for field widths of 4, 4.5 and 5 cm (cranial-caudal direction) (Figure 2D). Differently from the second experiment, shielded dose rates were taken by fully closing the shielding and measuring the dose rate on all detectors rather than just one.

To quantify the differences in dose rates (1) between irradiators; (2) between phantom and animals; (3) between surface and lung dose rates; and (4) shielded versus unshielded dose rates, dose rate measurements were appropriately grouped and depending on the number of available measurements either an unpaired Student's t-test (mice) or Wilcoxon rank-sum test (rats) was used for significance testing. Differences resulting in p-values less than 0.05 were considered significant.

RESULTS

Field uniformity

Figures 3A–C represent the following dose distributions taken on Irradiator A: (1) the entire exposed film normalized to the maximum recorded net pixel value, (2) horizontal and vertical 1D profiles across the 25%, 50% and 75% points in this normalized field and (3), the dose distributions of the useable field normalized to the mean pixel value within this field. Figures 3D–F represents the same measurements for Irradiator B. The relatively flat profiles across the field seen in Figures 3B and 3F indicate excellent field uniformity. There are small areas of higher intensity relative to the mean pixel value, but they are only6% higher for Irradiator A (Figure 3C) and 4% for Irradiator B (Figure 3F). Irradiator A and Irradiator B useable fields showed minimum PVs of 51% and 55% lower than the mean. Both minimums are located at the lower right extreme edge of the image. This indicates these minimums are caused by how the rectangular ROI was defined and at this extreme edge of the image no animals would be located at this point of the useable field. The overall variation throughout this useable field is also low, with the relative standard deviation of all pixel values equal to 3.5% for Irradiator A and 4.4% for Irradiator B.

Figure 4 shows the dose distributions resulting from two different field widths created by the addition of shielding; the figure includes both the 2D dose distributions and 1D profiles for each field width that were used. The number of pixels lying between the 50% relative intensity level were converted to a physical distance using the fact the film was scanned at a resolution of 71 dpi. For the 1.5 cm field the number of pixels that were counted was 44 ± 2 corresponding to a field size of 1.57 ± 0.07 cm and for the 4 cm field size measurements 120 ± 2 pixels were counted corresponding to a field size of 4.30 ± 0.07 cm. The slight increase in field size measured using the film can be attributed to geometric beam divergence due to the distance between the lead shielding and film. Given that the source-to-shield distance is 70 cm and the source-to-film distance is 75 cm, for a field size of 1.5 cm set by the lead shielding, the theoretical field size on the film would be (75÷70) × 1.5 = 1.61 cm. Similarly, for a 4 cm field size, the theoretical field size on the film is 4.28 cm. Therefore, the measured field widths from the profiles agree with the field sizes measured during setup.

Dose rates

Dose rate consistency results shown in Table 1 indicate that for both irradiators the total dose recorded by the MOSFETs and the planned 10 Gy dose differ by less than 5% (50 cGy). Table 1 also indicates that the irradiation times required to deliver a 10 Gy total dose were longer than 10 minutes and therefore an order of magnitude longer than the 30 second or 1 minute MOSFET measurements; we consider this a long irradiation time.

Mean mice lung dose rates shown in Table 2 were 72.2 ± 7.5 cGy min^{-1} and 73.8 ± 10.7 cGy min^{-1} measured on Irradiator A and B, respectively. The difference was not statistically significant (Student's t-test, p=04540) so mice lung dose rate measurements from these irradiators were pooled. Using the mice from Irradiator A as an example, and assuming a normal distribution, the 95% confidence interval for lung dose rate is 69.7 to 74.6 cGy/min, which leads to a range of total absorbed doses of 14.5–15.4 Gy for a hypothetical 15 Gy desired total dose.

The mean dose rate for the mouse phantom lung measurements (78.3 ± 7.4 cGy min^{-1}) was significantly different (Student's t-test, p=0.0059) from the mean dose rate of the in-animal lung measurements (72.9 ± 9.2 cGy min^{-1}). Mean rat phantom lung dose rates (81.8.± 3.9 cGy min^{-1}) were also significantly different (Wilcoxon rank-sum, p=0.0005) from in-animal measurements (75.1 ± 2.9 cGy min^{-1}) (Table 2). The consistently higher dose rates measured in the thoracic region of the phantoms versus animals indicate that the phantoms are not a precise representation of animal dose rates. Differences in anatomy between the phantom and animals such as the lack of skin, muscle, and ribs of a real animal could be responsible.

For mice, the difference in mean surface dose rate (86.8 ± 8.7 cGy min^{-1}) compared to lung dose rate (72.9 ± 9.2 cGy min^{-1}) was significant (Student's t-test, p<0.0001). For rats, the difference in mean surface dose rate (95.2 ± 2.8 cGy min^{-1}) compared to mean lung dose (75.1 ± 2.9 cGy min^{-1}) was also significant (Wilcoxon rank-sum, p<0.0001) (Table 2).

Shielding transmission factors were low with mean value of 4.1 ± 1.4%. Interestingly, the transmission factor varied with animal as the phantom, mice and rat transmission factors were 3.2%, 5.1% and 4.1%, respectively (Table 3). The mean transmission factor of 4.1% corresponds to a mean dose rate of 3.4 cGy min^{-1} under the shielding. This agrees with the design calculations within the uncertainties and when dose rates of close to 1 Gy min^{-1} are intended to be delivered to target organs we consider the dose that does reach those shielded parts of the animals to be acceptable.

Discussion

A key part of the development of medical countermeasures for the treatment of radiation induced tissue toxicities is creating valid animal models of human radiation injury through which the efficacy of proposed therapeutic agents can be tested (Stone et al. 2004, Augustine et al. 2005, DiCarlo et al. 2008, Williams et al. 2010). To ensure consistent testing and the ability to draw accurate comparisons among findings, a part of this model should include in depth characterization of the radiation parameters in use at various facilities. Here, we introduce a novel small animal irradiation platform (SAIP) to be used in conjunction with orthovoltage x-ray irradiators. In evaluating the performance of this platform, we examined a set of parameters that provided information about the true delivery of radiation to target organs, specifically the lung. We feel that these measurements should be used to advise the radiation setups and dosimetry used in future radiation research to improve accuracy and reliability.

When irradiating specific organs or regions of an animal it is important to have an accurately defined field size and uniform delivery of radiation. Uneven dose distribution and accidental irradiation beyond a specified field, particularly on a small animal, could result in unintended organ damage, leading to inaccurate conclusions. Using radiochromic film, we measured the actual field size and uniformity for several measured apertures commonly used in our delivery of radiation. We found no significant deviations in field uniformity of the two orthovoltage irradiators tested (Figure 3). Not surprisingly, we did observe a discrepancy between the set field sizes and those measured using film (Figure 3). However, this is geometric beam divergence and a simple calculation accounting for the difference in source-to-shield distance and source-to-film distance can be used to adjust the field size. Depending on a particular shielding design such adjustments may be crucial to ensure the correct field size, and hence, dose-rate is being delivered and in the desired region of all animals being irradiated.

We found the shielding transmission factors to be low, but did observe that transmission varied for phantoms, rats, and mice (Table 3). This is likely due to the differences in phantom, mouse and rat size anatomy both causing different scatter effects and affecting our ability to place the detectors at exactly the same source-to-detector distance for all measurements. For our purposes, the dose rate to shielded areas is acceptably low but proper shielding design should be undertaken for any investigators considering a new small animal irradiation platform.

The total radiation dose received by an animal, as well as the response of the irradiated tissues, is dependent on the dose rate of administration (Barendsen 1982). For this reason, it is important to establish a constant dose rate both within and between experiments. Irradiating MOSFET detectors for durations that were calculated in order to deliver 10 Gy resulted in differences of less than 5%. This illustrates two related points: first, shorter and easy to acquire dose-rates measurements are accurate enough to plan radiation doses delivered over long beam-on times and second, the orthovoltage irradiators have linear dose rate output over the longer exposure times used in this study. Further, any discrepancies in total dose can be explained by a decrease in the MOSFET detector calibration factor (CF) observed in multiple studies (Ehringfeld et al. 2005, Tremblay et al. 2005, Lavallee et al. 2006). Even given this behavior, the use of MOSFET detectors is still preferred to thermo luminescent detectors (TLD) for three reasons: first, the setup and processing time involved with TLDs is much greater than with MOSFET detectors; second, TLDs lack the ability to provide near-real time dose rate measurements; and third, the performance and accuracy of TLDs compared to MOSFET are closely comparable (Yoshizumi et al. 2007, De Lin et al. 2008).

Though these technical validations provide useful insight about the performance of this platform, it is also necessary to assess radiation delivery to the desired animal model, as absorption may differ within tissues (Beyer et al. 2008). We accomplished this using both tissue equivalent phantoms and euthanized animals with implanted MOSFET detectors. This allowed us to verify radiation doses in animal tissue and assess the accuracy of the phantom as an animal proxy for dosimetry measurements. The total dose measured in the thoracic region of the phantom was consistently higher than that measured in the lung of the

euthanized animals. With excellent field uniformity, we feel that the higher dose rates measured in the phantom are indicative that the differences between our phantom and animals, such as the lack of lung, ribs and muscle, or larger animal sizes are responsible for differences in beam attenuation, and hence dose rate. As we would expect, we observed a reduction in dose rate in the lung compared to the entrance dose rate in both phantoms and animals. These observations indicate that researchers should use caution when relying solely on phantoms for dosimetry, as this may not be an accurate measure of the dose received in a living animal. Furthermore, the precision in dose rates measurements must be considered when planning small animal radiation studies. With sources of uncertainties originating from the MOSFET detectors, field uniformity, anatomy variation and animal positioning, such considerations are crucial to ensure each animal cohort is in a specific dose level group and to account for strains showing sharp dose-responses due to enhanced radiation sensitivity. Our example of a hypothetical 15 Gy dose showed that we can achieve a range of doses within 1 Gy but this may not be precise enough for some drug studies. Therefore, additional dosimetry or power calculations to estimate the number of animals required, taking into consideration the variability in dose-rate during each run may be prudent when screening medical countermeasures.

In summary, our SAIP improves upon previous systems by permitting localized irradiation of multiple animals at once. This will improve the efficiency of large scale animal studies that will be necessary to screen potential medical countermeasures for radiation exposure. In developing this system we examined field uniformity, field size, dose rate consistency, and efficacy of shielding. We also examined the difference in dose rate experienced between phantoms and euthanized animals, as well as the discrepancy in rate at tissue surfaces versus target organs. These measurements are important, as they allow us to better determine the nature of the experimentally inflicted radiation injury in a small animal model. Measurement of these parameters by all institutions, using any irradiation system, could improve the ability of researchers to compare findings. Establishment of this level of consistency will increase the capacity for high throughput screening of therapeutic agents, expediting the development of effective countermeasures for radiation induced tissue injury.

ACKNOWLEDGEMENTS

This project has been funded in whole or in part with Federal funds from the National Institute of Allergy and Infectious Diseases, National Institutes of Health, Department of Health and Human Services, under Contract No. HHSN266200500043C."

REFERENCES

Augustine AD, Gondré-Lewis T, McBride W, Miller L, Pellmar TC, Rockwell S. Animal models for radiation injury, protection and therapy. Radiation Research. 2005; 164:100–109. [PubMed: 15966769]

Barendsen GW. Dose fractionation, dose rate and iso-effect relationships for normal tissue responses. Int J Radiat Oncol Biol Phys. 1982; 8:1981–1997. [PubMed: 6759484]

Berger M, Hubbell J, Seltzer S, Chang J, Coursey J, Sukumar R, Zucker D, Olsen K. Xcom: Photon cross sections database (nist). 1998

Beyer GP, Mann GG, Pursley JA, Espenhahn ET, Fraisse C, Godfrey DJ, Oldham M, Carrea TB, Bolick N, Scarantino CW. An implantable mosfet dosimeter for the measurement of radiation dose in tissue during cancer therapy. Sensors Journal, IEEE. 2008; 8:38–51.

Blair A, Meyer J. Characteristics of gafchromic xr-rv2 radiochromic film. Med Phys. 2009; 36:3050–3058. [PubMed: 19673204]

Clarkson R, Lindsay PE, Ansell S, Wilson G, Jelveh S, Hill RP, Jaffray DA. Characterization of image quality and image-guidance performance of a preclinical microirradiator. Medical Physics. 2011; 38:845–856. [PubMed: 21452722]

Coleman CN, Stone HB, Moulder JE, Pellmar TC. Modulation of radiation injury. Science. 2004; 304:693–694. [PubMed: 15118152]

De Lin M, Toncheva G, Nguyen G, Kim S, Anderson-Evans C, Johnson GA, Yoshizumi TT. Application of mosfet detectors for dosimetry in small animal radiography using short exposure times. Radiation Research. 2008; 170:260–263. [PubMed: 18666818]

DiCarlo AL, Hatchett RJ, Kaminski JM, Ledney GD, Pellmar TC, Okunieff P, Ramakrishnan N. Medical countermeasures for radiation combined injury: Radiation with burn, blast, trauma and/or sepsis. Report of an niaid workshop, march 26–27, 2007. Radiation Research. 2008; 169:712–721. [PubMed: 18494548]

Ehringfeld C, Schmid S, Poljanc K, Kirisits C, Aiginger H, Georg D. Application of commercial mosfet detectors for in vivo dosimetry in the therapeutic x-ray range from 80 kv to 250 kv. Phys Med Biol. 2005; 50:289–303. [PubMed: 15742945]

Lavallee MC, Gingras L, Beaulieu L. Energy and integrated dose dependence of mosfet dosimeter sensitivity for irradiation energies between 30 kv and 60co. Med Phys. 2006; 33:3683–3689. [PubMed: 17089834]

Ma CM, Coffey CW, DeWerd LA, Liu C, Nath R, Seltzer SM, Seuntjens JP. Aapm protocol for 40–300 kv x-ray beam dosimetry in radiotherapy and radiobiology. Med Phys. 2001; 28:868–893. [PubMed: 11439485]

McLaughlin WL, Yun-Dong C, Soares CG, Miller A, Van Dyk G, Lewis DF. Sensitometry of the response of a new radiochromic film dosimeter to gamma radiation and electron beams. Nuclear Instruments and Methods in Physics Research Section A: Accelerators, Spectrometers, Detectors and Associated Equipment. 1991; 302:165–176.

Newton J, Oldham M, Thomas A, Li Y, Adamovics J, Kirsch DG, Das S. Commissioning a small-field biological irradiator using point, 2d, and 3d dosimetry techniques. Med Phys. 2011; 38:6754–6762. [PubMed: 22149857]

Ngwa W, Korideck H, Chin LM, Makrigiorgos GM, Berbeco RI. Mosfet assessment of radiation dose delivered to mice using the small animal radiation research platform (sarrp). Radiation Research. 2011; 176:816–820. [PubMed: 21962005]

Ngwa W, Korideck H, Chin LM, Makrigiorgos GM, Berbeco RI. Mosfet assessment of radiation dose delivered to mice using the small animal radiation research platform (sarrp). Radiat Res. 2011; 176:816–820. [PubMed: 21962005]

Pellmar TC, Rockwell S. Priority list of research areas for radiological nuclear threat countermeasures. Radiation Research. 2005; 163:115–123. [PubMed: 15606315]

Scarantino CW, Ruslander DM, Rini CJ, Mann GG, Nagle HT, Black RD. An implantable radiation dosimeter for use in external beam radiation therapy. Medical Physics. 2004; 31:2658–2671. [PubMed: 15487749]

Stojadinovic S, Low DA, Hope AJ, Vicic M, Deasy JO, Cui J, Khullar D, Parikh PJ, Malinowski KT, Izaguirre EW, Mutic S, Grigsby PW. Micrort---small animal conformal irradiator. Medical Physics. 2007; 34:4706–4716. [PubMed: 18196798]

Stone HB, Moulder JE, Coleman CN, Ang KK, Anscher MS, Barcellos-Hoff MH, Dynan WS, Fike JR, Grdina DJ, Greenberger JS, Hauer-Jensen M, Hill RP, Kolesnick RN, Macvittie TJ, Marks C, McBride WH, Metting N, Pellmar T, Purucker M, Robbins ME, Schiestl RH, Seed TM, Tomaszewski JE, Travis EL, Wallner PE, Wolpert M, Zaharevitz D. Models for evaluating agents intended for the prophylaxis, mitigation and treatment of radiation injuries. Report of an nci workshop, december 3–4, 2003. Radiat Res. 2004; 162:711–728. [PubMed: 15548121]

Tremblay C, Gingras L, Archambault L, Chretien M, Martin A, Roy R, Beaulieu L. Characterization and use of mosfet as in vivo dosimeters under 192ir irradiation for real-time quality assurance. Medical Physics. 2005; 32:2003–2003.

Verhaegen F, Granton P, Tryggestad E. Small animal radiotherapy research platforms. Phys Med Biol. 2011; 56:R55–R83. [PubMed: 21617291]

Williams JP, Brown SL, Georges GE, Hauer-Jensen M, Hill RP, Huser AK, Kirsch DG, Macvittie TJ, Mason KA, Medhora MM, Moulder JE, Okunieff P, Otterson MF, Robbins ME, Smathers JB, McBride WH. Animal models for medical countermeasures to radiation exposure. Radiat Res. 2010; 173:557–578. [PubMed: 20334528]

Wong J, Armour E, Kazanzides P, Iordachita I, Tryggestad E, Deng H, Matinfar M, Kennedy C, Liu Z, Chan T, Gray O, Verhaegen F, McNutt T, Ford E, DeWeese TL. High-resolution, small animal radiation research platform with x-ray tomographic guidance capabilities. Int J Radiat Oncol Biol Phys. 2008; 71:1591–1599. [PubMed: 18640502]

Yoshizumi T, Brady SL, Robbins ME, Bourland JD. Specific issues in small animal dosimetry and irradiator calibration. Int J Radiat Biol. 2011; 87:1001–1010. [PubMed: 21961967]

Yoshizumi TT, Goodman PC, Frush DP, Nguyen G, Toncheva G, Sarder M, Barnes L. Validation of metal oxide semiconductor field effect transistor technology for organ dose assessment during ct: Comparison with thermo luminescent dosimetry. AJR Am J Roentgenol. 2007; 188:1332–1336. [PubMed: 17449779]

Zhou H, Rodriguez M, van den Haak F, Nelson G, Jogani R, Xu J, Zhu X, Xian Y, Tran PT, Felsher DW, Keall PJ, Graves EE. Development of a micro-computed tomography–based image-guided conformal radiotherapy system for small animals. International Journal of Radiation Oncology*Biology*Physics. 2010; 78:297–305.

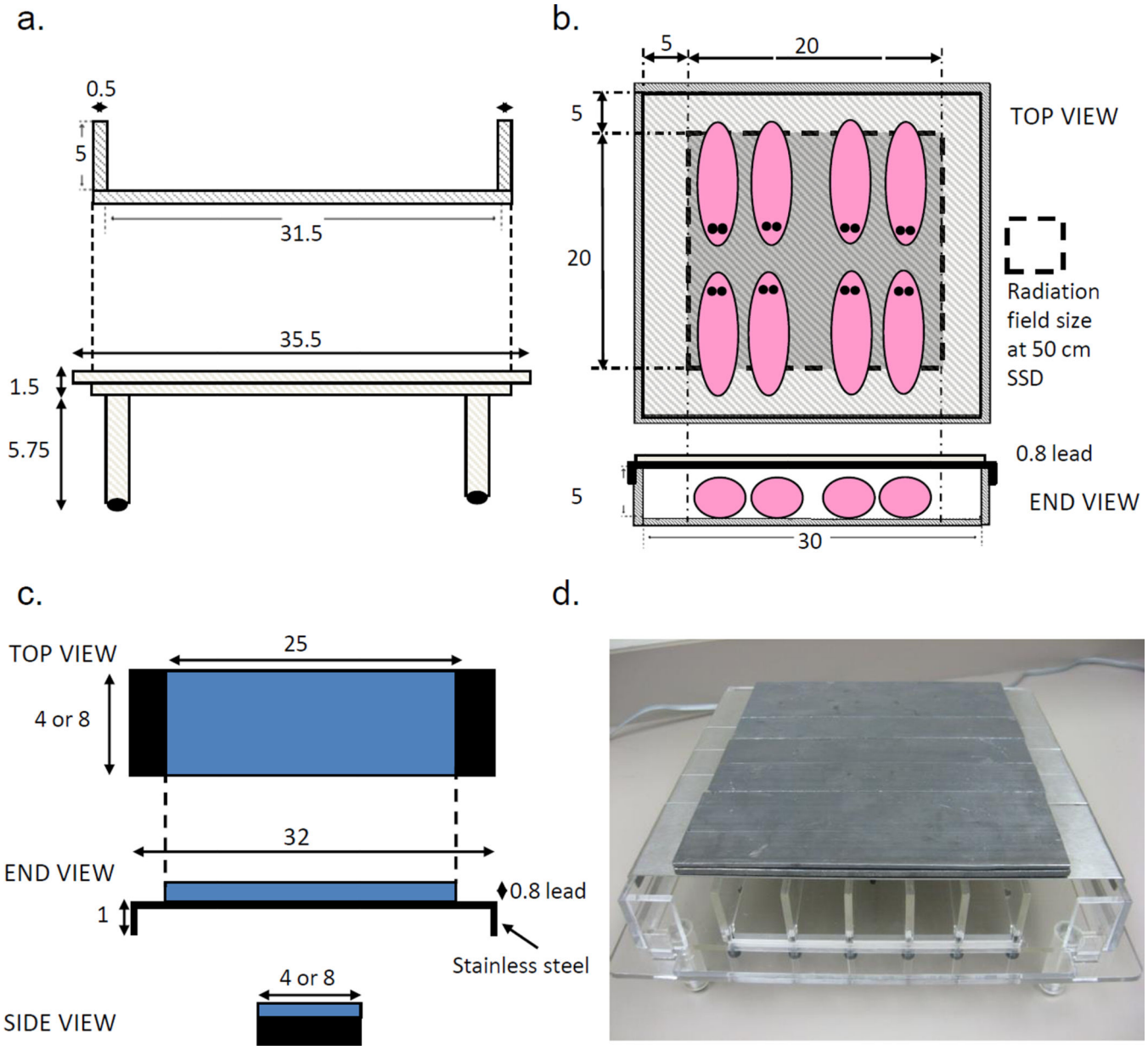

Figure 1.

Small animal radiation platform design. A) The end on view of the platform base. B) Top-down (beam's-eye) view of platform showing dimensions of the radiation field at 50 cm SSD and example positions of animals. C) Lead shielding design with top, end and side views. D) Photo of assembled platform. All dimensions are in cm.

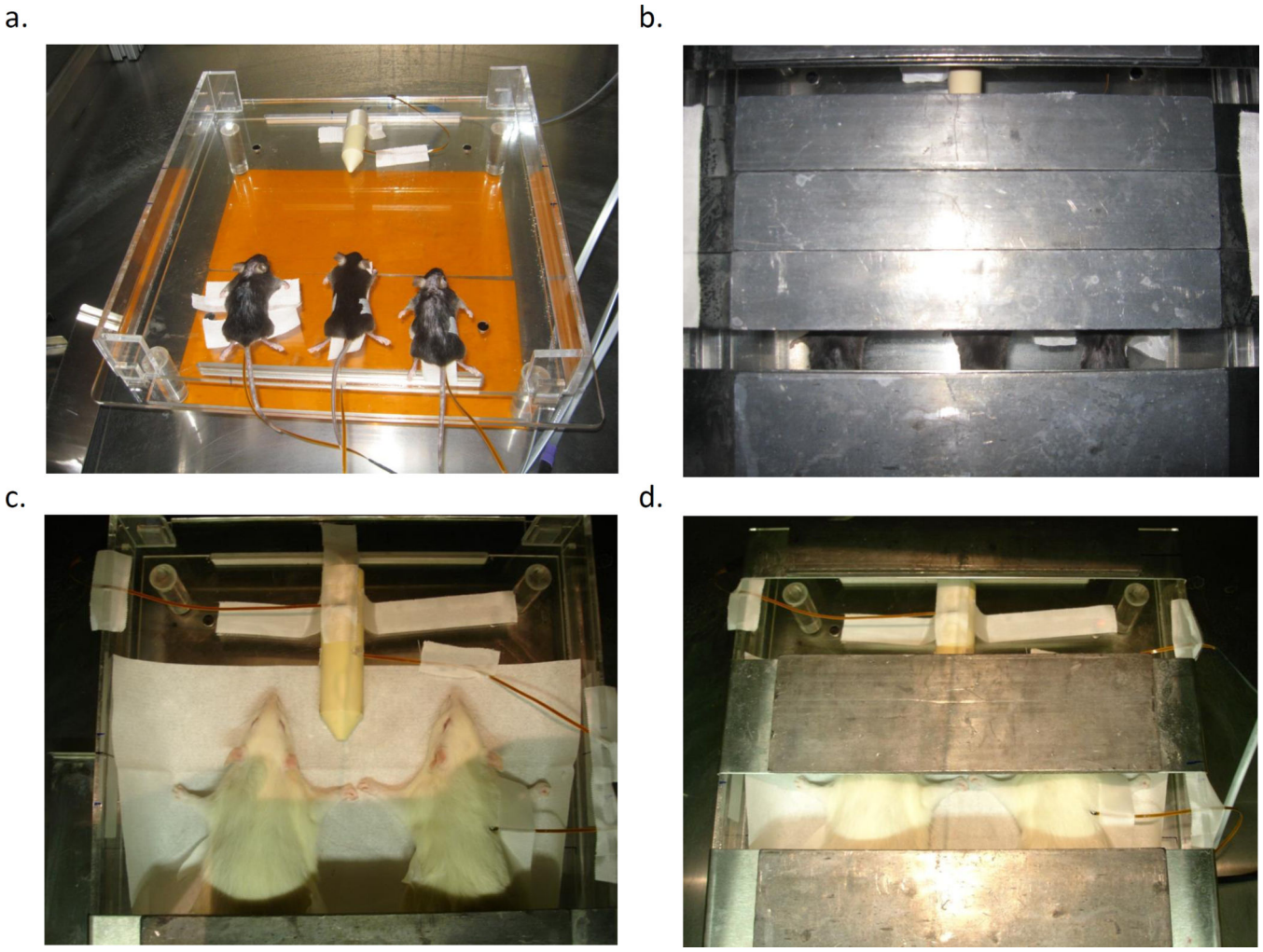

Figure 2.

Experimental setup for dose rate measurements. A) Mice dosimetry experiment with mice 1–3 closest to camera and phantom on opposite side of base. Orange film below platform is the Gafchromic film used for MOSFET localization. B) Mice dosimetry experiment with 1.5 cm field size for whole-thorax irradiation. C) Rat dosimetry experiment with two Wistar rats with MOSFETS inserted into thoracic cavity and rat phantom opposite. Note the presence of the MOSFET detectors on the phantom and rat skin for skin dose measurements. D) Rat dosimetry experiment with field size set to 4 cm for both rats and phantoms.

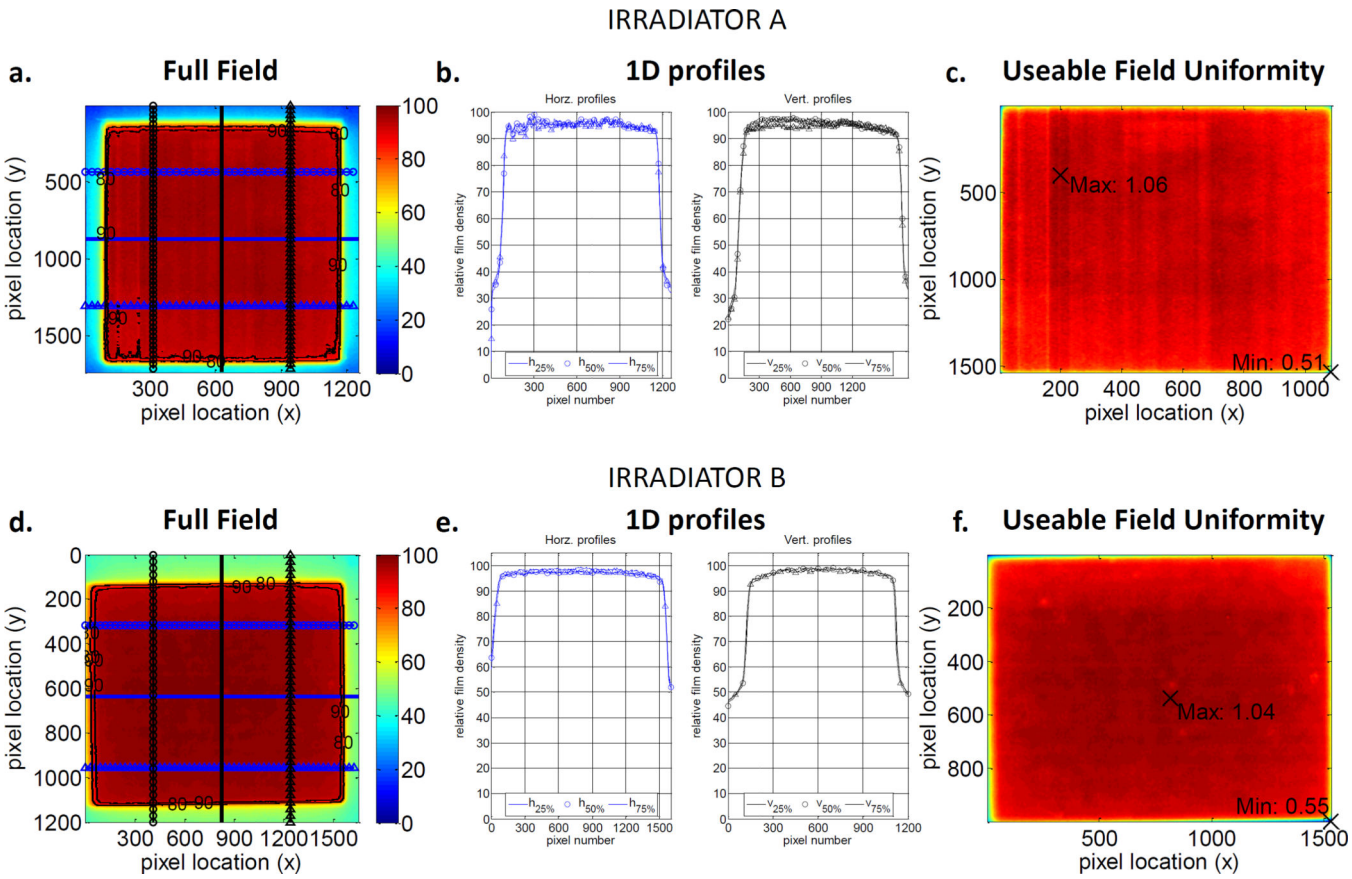

Figure 3.

Field uniformity results for Irradiator A (A–C) and Irradiator B (D–F) XRAD-320 kilovoltage irradiators. Images A and D represent pixel values of the whole field normalized to the maximum pixel value. B and D are 1D profiles 25%, 50% and 75% across this normalized field in the horizontal and vertical directions. C and F show the variation in pixel values within the useable field normalized to the mean value.

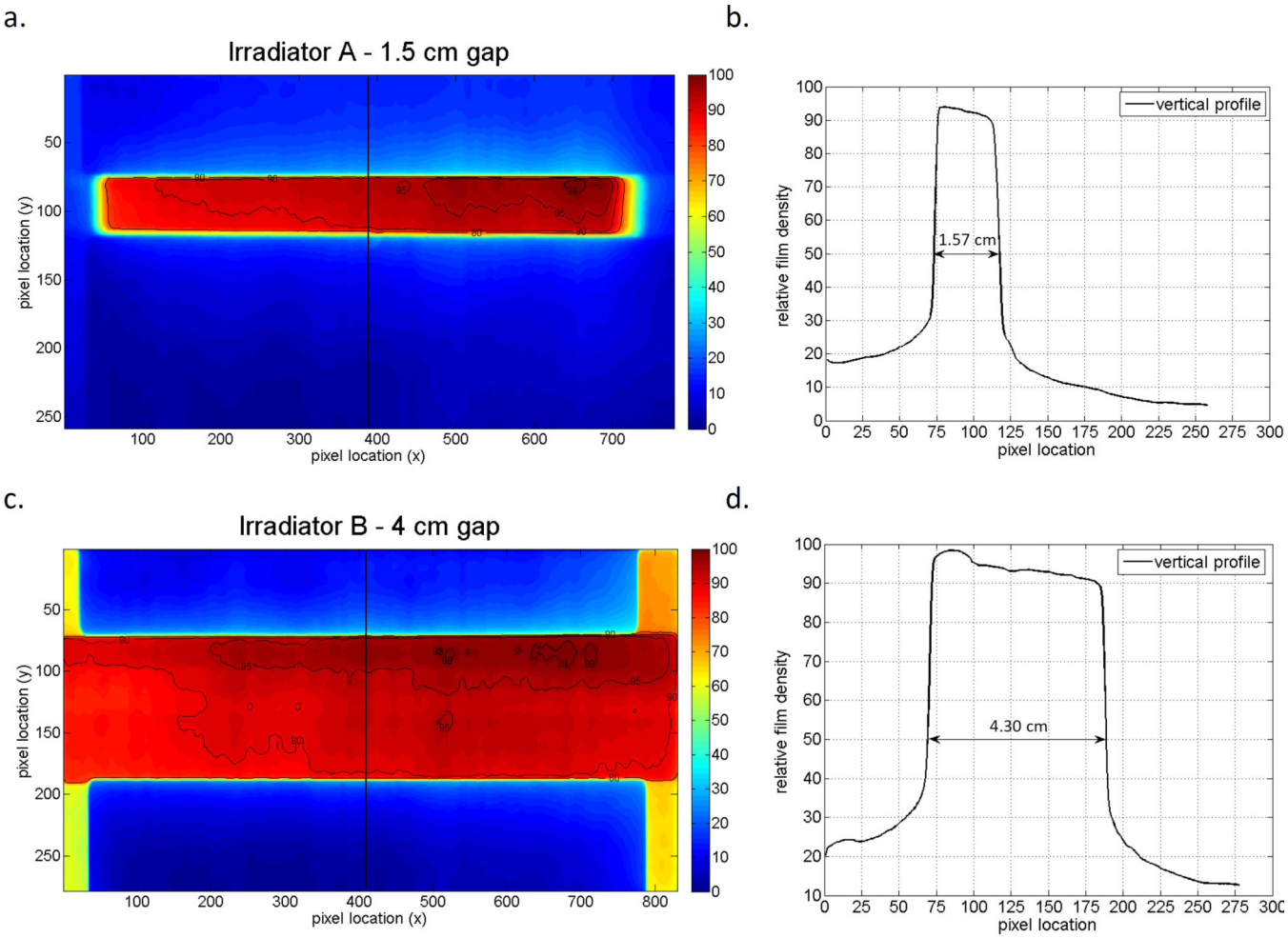

Figure 4.

A) 2D intensity distributions relative to maximum net pixel value, B) Transverse profile across the field for the 1.5 cm field size defined using the lead shield for irradiator A. C) 2D intensity distributions relative to maximum net pixel value and, D) transverse profile across the field for the 4.0 cm field size defined using the lead shield for irradiator B. Note that the radiation field size is defined as the distance between the 50% relative intensity line (indicated by the arrows in Fig B and D).

Table 1

Dose rate consistency test results for 1.5 cm and open field sizes.

Irradiator		Average dose rate [cGy/min]	Time to deliver 1000 cGy [min]	Average recorded dose after delivered time [cGy]	% difference
A	(1.5 cm field)	69.2	14.5	965	−3.6
B	(open field)	91.2	11.0	958	−4.2

Table 2

Comparison of phantom and in-animal mean dose-rate measurements. Dose rates from all field sizes (1, 1.5, 2 and 30 cm) have been pooled. Parentheses note the number of measurements used in each comparison.

Comparison	Mean Dose Rate [cGy/min]		p-value
In-animal (mice) lung dose rate - Irradiator A (col. 2) and Irradiator B (col. 3)	72.2 ± 7.5 (39)	73.8 ± 10.7 (36)	0.4540
Phantom dose rate (col 2.) and in-animal (mice) lung dose rate (col. 3)	78.3 ± 7.4 (13)	72.9 ± 9.2 (75)	0.0059*
Phantom dose rate (col. 2) and in-animal (rats) lung dose rate (col.3)	81.8. ± 3.9 (9)	75.1 ± 2.9 (18)	0.0005*
Entrance dose rate (col. 2) and lung dose rate (mice) (col. 3)	86.8 ± 8.7 (12)	72.9 ± 9.2 (75)	<0.0001*
Entrance dose rate (col. 2) and lung dose rate (rats) (col. 3)	95.2 ± 2.8 (9)	75.1 ± 2.9 (18)	<0.0001*

*Wilcoxon rank sum test used for significance testing due to fewer subjects in each group. However, mean and standard deviations are still reported for consistency.

Table 3

Shielding transmission measurements indicated as the mean recorded dose rates (cGy min^{-1}) using (N) measurements

	Shielded	Exposed	%
Phantom	2.8 ± 1.6 (6)	86.9 ± 6.1 (18)	3.2 ± 1.3
Mice	4.1 ± 0.5 (6)	80.3 ± 11.8 (39)	5.1 ± 1.0
Rats	3.4 ± 0.6 (9)	81.8 ± 10.1 (27)	4.1 ± 0.9
Overall	3.4 ± 1.1 (21)	82.2 ± 10.5 (84)	4.1 ± 1.4